THE JOURNAL OF PHYSICAL CHEMISTRY A

 VOLUME 113, NUMBER 25, JUNE 25, 2009

ARTICLES

Quantum State Distribution of the OH $X^2\Pi$ Products from Collisional Quenching of OH $A^2\Sigma^+$ by O_2 and CO_2

Logan P. Dempsey, Timothy D. Sechler, Craig Murray,[†] and Marsha I. Lester*

Department of Chemistry, University of Pennsylvania, Philadelphia, Pennsylvania 19104-6323

Received: March 31, 2009; Revised Manuscript Received: May 6, 2009

The OH $X^2\Pi$ product state distribution arising from quenching of electronically excited OH $A^2\Sigma^+$ by O_2 and CO_2 under single collision conditions has been determined using a pump−probe technique. For both collision partners, the majority of OH $X^2\Pi$ products are observed in their lowest vibrational level, $v'' = 0$, with significantly less population in $v'' = 1$. The OH products from quenching by O_2 are generated with a substantial degree of rotational excitation, peaking around $N'' \approx 17$, with an average rotational energy of ~4800 cm^{-1}, whereas OH products from quenching by CO_2 exhibit a moderate degree of rotational excitation, peaking around $N'' \approx 5$, with an average rotational energy of ~1800 cm^{-1}. The branching fraction into OH $X^2\Pi$ products states reveals that nonreactive quenching is a significant decay pathway for both systems, accounting for at least 40(1)% of the quenched products with O_2 and 64(5)% with CO_2.

I. Introduction

Hydroxyl radicals are important in both atmospheric and combustion environments,[1,2] where they are often detected by laser-induced fluorescence (LIF) on the $A^2\Sigma^+ - X^2\Pi$ band system.[3] Collisional quenching of electronically excited OH $A^2\Sigma^+$ affects the LIF measurements and, as such, has attracted much attention in the literature. The majority of studies on collisional quenching of OH $A^2\Sigma^+$ by various molecular partners (M) have focused on measuring quenching rates and/or cross sections and their dependence on temperature and initial OH $A^2\Sigma^+$ rovibrational level.[4−10] In general, quenching rates have been found to decrease with increasing temperature, indicating that attractive forces govern the kinetics. Quenching rates also decrease with increasing OH $A^2\Sigma^+$ rotational level, suggesting that certain orientations of OH with respect to the collision partner preferentially lead to quenching. The latter has been attributed to the anisotropy of the OH $A^2\Sigma^+ + M$ intermolecular potential energy surfaces. For example, collisional quenching of OH $A^2\Sigma^+$ by O_2 and CO_2 are efficient processes with room-temperature cross sections of ~20 and ~60 $Å^2$, respectively,[4−6,8−12] and show the typical dependences on temperature and initially prepared OH $A^2\Sigma^+$ rotational level.

Despite extensive kinetic measurements, there is little known about the mechanism by which molecules are collisionally quenched or the outcomes of such events.[13] A variety of empirical models have been proposed to explain the trends observed in kinetics studies, in particular, the magnitude and temperature dependence of the quenching cross sections.[4,12,14−17] Nevertheless, high-level theoretical studies of quenching are available for OH $A^2\Sigma^+$ with only a few partners, namely, H, H_2, and N_2.[18−23] Collisional quenching of electronically excited OH $A^2\Sigma^+$ can occur through two types of processes:

* To whom correspondence should be addressed. Tel: (215) 898-4640. Fax: (215) 573-2112. E-mail: milester@sas.upenn.edu.
[†] Current address: School of Chemistry, University of Bristol, Bristol BS8 1TS, U.K.

10.1021/jp902935c CCC: $40.75
Published on Web 05/29/2009

nonreactive quenching that returns OH $A^2\Sigma^+$ population to its ground $X^2\Pi$ electronic state and reaction. The former is fundamentally a nonadiabatic process, whereas the latter need not be. The outcomes for collisional quenching of OH $A^2\Sigma^+$ by H_2/D_2 and N_2 partners have been studied extensively. For both systems, the reactive[24−27] and nonreactive[22,23,28−30] quenching processes have been investigated experimentally. Similar types of studies have examined the vibrational distribution of NO $X^2\Pi$ from collisional quenching of NO $A^2\Sigma^+$ by various molecular partners.[31,32] This article expands experimental studies on the outcomes of collisional quenching of OH $A^2\Sigma^+$ to include quenching by O_2 and CO_2. Background information on the OH $A^2\Sigma^+ + O_2$ and CO_2 systems follows after a summary of work on quenching of OH $A^2\Sigma^+$ by H_2/D_2 and N_2.

Quenching of OH $A^2\Sigma^+$ by H_2 can take place through a reactive pathway, producing $H_2O + H$ ($\Delta E = -4.66$ eV), and a nonreactive pathway, producing OH $X^2\Pi + H_2$ ($\Delta E = -4.02$ eV). Ab initio calculations of the interaction between H_2 and OH in its ground $X^2\Pi$ and excited $A^2\Sigma^+$ states have shown that quenching is facilitated by regions of conical intersection (CI) that occur in configurations in which the oxygen side of OH points toward H_2.[19,20,22,33]

The reactive channel was initially investigated by Lester and coworkers with H_2 and D_2 collision partners, where studies revealed that a large fraction of the available energy is partitioned into internal excitation of the water product.[24,25] Reactive quenching of OH $A^2\Sigma^+$ by D_2 was reinvestigated by the Davis group in a crossed molecular beam scattering experiment, which showed the D atoms to be mostly forward scattered, indicating a direct reaction mechanism.[27]

More recent experiments have characterized the nonreactive quenching pathway by examining the OH $X^2\Pi$ product state distribution (PSD).[22,28−30] OH $X^2\Pi$ products are generated primarily in their lowest vibrational level, $v'' = 0$, with significantly less population in higher vibrational levels. Most strikingly, the OH $X^2\Pi$ ($v'' = 0$) products exhibit a high degree of rotational excitation, peaking around $N'' = 15$, and a strong propensity for $p\pi$ orbital alignment, as indicated by a strong preference for the $\Pi(A')$ Λ-doublet component. The latter observations were interpreted to arise from a large torque placed on OH as the system evolves through the CI region and the A' symmetry of the states forming the CI.[19] The branching between the nonreactive and reactive pathways was also determined, and reactive quenching was found to be the dominant pathway, accounting for 88(5)% of quenched products.[29]

Quenching of OH $A^2\Sigma^+$ by N_2 has also been investigated, allowing interesting comparisons to be made with H_2, with which there are many similarities. An energetically accessible CI leading to nonreactive quenching ($\Delta E = -4.02$ eV) has been located theoretically.[20] In addition, a reactive channel producing $H + N_2O$ products ($\Delta E = -1.03$ eV) is potentially open but has not been observed in experimental or theoretical studies.[23,27] As a result, recent experiments focused on characterizing the OH $X^2\Pi$ products from nonreactive quenching.[23] The OH $X^2\Pi$ products are generated predominantly in $v'' = 0$ and display a significant degree of rotational excitation in a broad distribution that peaks around $N'' = 18$, with a moderate propensity for the $\Pi(A')$ Λ-doublet component. Whereas the OH $X^2\Pi$ PSD shows similarities to that observed with H_2, the branching fraction is markedly different, with more than 88% of quenching events resulting in nonreactive products. The rotational excitation of the OH $X^2\Pi$ products and branching fraction were understood with the help of complementary calculations characterizing the topography of the CI region. These calculations revealed a tilt of the cone that favors nonreactive quenching and an interstate coupling vector that puts a large torque on the OH radical.

This work extends previous studies by examining the outcomes of OH $A^2\Sigma^+$ quenching by other important collision partners found in combustion and atmospheric environments, namely O_2 and CO_2. These systems are more complex than those previously studied because they exhibit multiple low-lying electronic states, reactive channels, or both.[34] Quenching of OH $A^2\Sigma^+$ by O_2 can occur through nonreactive pathways, producing OH in its $X^2\Pi$ state and O_2 in any of several low-lying electronic states

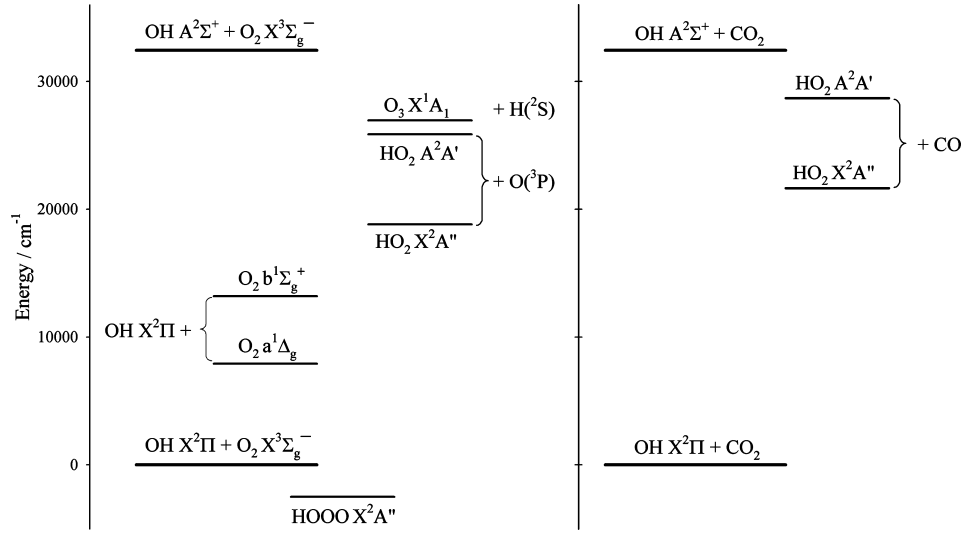

Figure 1. Schematic energy level diagram illustrating the initially prepared excited OH $A^2\Sigma^+$ electronic state that is quenched in collisions with O_2 and CO_2. For O_2, quenching produces OH in its ground $X^2\Pi$ electronic state and O_2 in its ground $X^3\Sigma_g^-$ state or low-lying electronic states. Reactive quenching can lead to $HO_2 + O$ and $O_3 + H$ products. For CO_2, nonreactive quenching produces OH $X^2\Pi + CO_2$, whereas reactive quenching can generate $HO_2 + CO$ products.

$$OH\ A^2\Sigma^+ + O_2\ X^3\Sigma_g^- \rightarrow OH\ X^2\Pi + O_2\ X^3\Sigma_g^- \quad \Delta E = -4.02\ eV$$
$$\rightarrow OH\ X^2\Pi + O_2\ a^1\Delta_g \quad \Delta E = -3.04\ eV$$
$$\rightarrow OH\ X^2\Pi + O_2\ b^1\Sigma_g^+ \quad \Delta E = -2.39\ eV$$

or though reactive channels

$$OH\ A^2\Sigma^+ + O_2\ X^3\Sigma_g^- \rightarrow HO_2\ X^2A'' + O(^3P) \quad \Delta E = -1.69\ eV$$
$$\rightarrow HO_2\ A^2A' + O(^3P) \quad \Delta E = -0.82\ eV$$
$$\rightarrow O_3\ X^1A_1 + H(^2S) \quad \Delta E = -0.68\ eV$$

We note that these reactions may be facilitated by the formation of an HOOO intermediate ($\Delta E = -4.33$ eV), which has been recently characterized.[35−38]

Quenching of OH $A^2\Sigma^+$ by CO_2 can occur through a nonreactive pathway

$$OH\ A^2\Sigma^+ + CO_2\ X^1\Sigma_g^+ \rightarrow OH\ X^2\Pi + CO_2\ X^1\Sigma_g^+ \quad \Delta E = -4.02\ eV$$

or through reaction

$$OH\ A^2\Sigma^+ + CO_2\ X^1\Sigma_g^+ \rightarrow HO_2\ X^2A'' + CO\ X^1\Sigma^+ \quad \Delta E = -1.34\ eV$$
$$\rightarrow HO_2\ A^2A' + CO\ X^1\Sigma^+ \quad \Delta E = -0.47\ eV$$

The energetically accessible outcomes for quenching of OH $A^2\Sigma^+$ by O_2 and CO_2 are depicted in Figure 1.[34] There has been no prior work, experimentally or theoretically, on the detailed outcomes of quenching by these partners. Here we report the OH $X^2\Pi$ PSD from quenching of OH $A^2\Sigma^+$ by O_2 and CO_2 as well as the branching fraction for OH $X^2\Pi$ production from nonreactive quenching.

II. Experimental Section

The methods for determining the OH $X^2\Pi$ PSD and branching fraction for nonreactive collisional quenching of OH $A^2\Sigma^+$ have previously been described in detail.[22,23,29,30] In the present case, a 20% O_2 or CO_2 balance He gas mixture is utilized as the carrier gas (150 psi); other aspects of the experimental method are unchanged. In brief, hydroxyl radicals are photolytically generated in the throat of a pulsed supersonic expansion. The quenching experiments are conducted in the collisional region of the expansion approximately $x/D = 5$ nozzle diameters downstream. A UV pump laser prepares OH radicals in the $v' = 0$, $N' = 0$ level of the excited $A^2\Sigma^+$ electronic state. After a 100 ns delay, a second counter-propagating and spatially overlapped UV laser is introduced to probe the quenched OH $X^2\Pi$ products on various OH $A^2\Sigma^+$−$X^2\Pi$ transitions with rovibrational (v'', N'') and fine-structure (F_n, ε) resolution. The following notation is utilized for OH $X^2\Pi$: vibrational level, v''; rotational level, N''; and the parity ε or associated Λ-doublet, $\Pi(A')$ or $\Pi(A'')$. The F_n label refers to the spin−orbit manifolds F_1 ($J = N + 1/2$) or F_2 ($J = N - 1/2$) for low rotational levels. However, the fairly rapid transition to Hund's case (b) and associated spin-decoupling in OH $X^2\Pi$ means that the splitting between F_n levels is dominated by spin-rotation coupling for higher rotational levels.

We obtained the PSDs by measuring the probe LIF intensities, initially scaled relative to a reference line, for each OH $X^2\Pi$ product state. Fluorescence lifetimes of the OH $A^2\Sigma^+$ (v', N') levels accessed by the probe transitions are also collected. The scaled intensities are converted to relative populations using a procedure described previously,[22] which also utilizes the fluorescence lifetimes and the detection sensitivity of the apparatus.

The branching fraction Γ_i is defined as the fraction of the collisionally quenched OH $A^2\Sigma^+$ population that appears in a particular OH $X^2\Pi$ (v'', N'', F_n, ε) product state, i. Γ_i can be related to the collision-induced population $P_{Q,i}$ of product state i relative to the population of the initially prepared OH $A^2\Sigma^+$ ($v' = 0$, $N' = 0$) state. Under saturated LIF conditions, the latter can be linked to the population in the OH $X^2\Pi_{3/2}$ ($v'' = 0$, $N'' = 1$, e) level, labeled $P_{X,N=1}$ through a degeneracy factor (1/3), and Γ_i can then be expressed in terms of experimental observables

$$\Gamma_i = \frac{P_{Q,i}}{\frac{1}{3}P_{X,N=1}(1 - \Phi_f)} \quad (1)$$

Here Φ_f is the fluorescence quantum yield. The denominator indicates the fraction of the initially prepared OH $A^2\Sigma^+$ ($v' = 0$, $N' = 0$) population that is collisionally removed; the balance decays radiatively. The population ratios, $P_{Q,i}/P_{X,N=1}$, are determined from the relative intensities of the pump and probe LIF signals[22] and are used to derive Γ_i for selected product states following an additional correction for the 100 ns pump−probe delay.

The experimental setup for branching fraction measurements is analogous to that utilized for measuring the OH $X^2\Pi$ PSD. However, different filter combinations (described previously[30]) were used to collect the pump and probe LIF signals, and a further correction was needed to account for differences in the photomultiplier detector gain settings. As an internal check, Γ_i was measured using two different pump LIF detection schemes, collecting fluorescence on the A−X (0,0) or (0,1) bands, and also for two different probe laser transitions. The relative LIF signal intensities were converted to branching fractions for each of these four measurements, and the results for each product state were averaged.

III. Results

A. Fluorescence Lifetimes. A marked reduction in the fluorescence lifetime, τ, of the OH $A^2\Sigma^+$ ($v' = 0$, $N' = 0$) level prepared by the pump laser when O_2 or CO_2 are present in the expansion is the most apparent indication that collisions induce quenching. The typical fluorescence lifetimes under our experimental conditions are 247(4) ns with O_2 and 187(24) ns with CO_2, which are significantly shorter than the radiative lifetime of ~700 ns.[39] Therefore, collision-induced quenching is the dominant decay process for OH $A^2\Sigma^+$ ($v' = 0$, $N' = 0$) population under these conditions, which is 3 to 4 times faster than radiative decay.

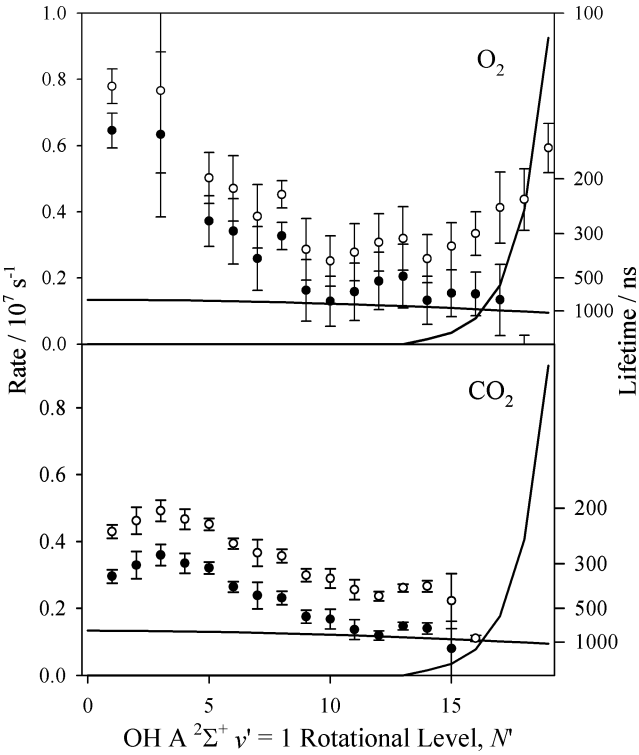

Figure 2. Pseudo-first-order decay rates and corresponding lifetimes for OH $A^2\Sigma^+$ ($v' = 1$) as a function of rotational level (N') for O_2 (upper panel) and CO_2 (lower panel). The experimentally observed total decay rates (k_{tot}, ○) along with radiative (k_{rad}, gray line) and predissociation (k_{PD}, black line) rates from ref 39 are used to derive collision-induced decay rates (k_{coll}, ●). The reported uncertainties for k_{tot} and k_{coll} are the standard deviations from repeated measurements.

Fluorescence lifetimes are also measured for each of the OH $A^2\Sigma^+$ (v', N') states accessed by the probe transitions. The fluorescence lifetimes are inversely related to total decay rates (k_{tot}), which are plotted as a function of OH $A^2\Sigma^+$ ($v' = 1$) rotational level in Figure 2. The removal rates for each N' level are an average of the F_1 and F_2 spin-rotation components as the observed fluorescence lifetimes agree within the uncertainty of the measurements. The total decay rate is the sum of collisional (k_{coll}), radiative (k_{rad}), and predissociation (k_{PD}) components

$$k_{tot} = k_{coll} + k_{rad} + k_{PD} \quad (2)$$

where the latter two quantities are obtained from the LIFBase tabulation.[39] Pseudo-first-order rates for collisional decay are determined using eq 2 and are shown in Figure 2. The radiative rate is fairly constant with N', whereas electronic predissociation increasingly contributes at high N' levels, becoming the dominant decay process at $N' \approx 17$. For both collision partners, the collisional decay rate (k_{coll}) under supersonic jet conditions (rotational temperature ~50 K) decreases with rotational excitation of OH $A^2\Sigma^+$ in a manner consistent with previous thermal studies.[4−9] An increase in the total decay rate at the highest rotational levels with O_2 as the collision partner is due to the onset of rapid electronic predissociation; these rotational levels were not accessed with CO_2 because of the less-extensive rotational excitation of the OH $X^2\Pi$ products from quenching.

The collisional contribution to the rate constant for the removal of OH $A^2\Sigma^+$ ($v' = 1$, N') can potentially include additional processes, such as vibrational energy transfer (VET).

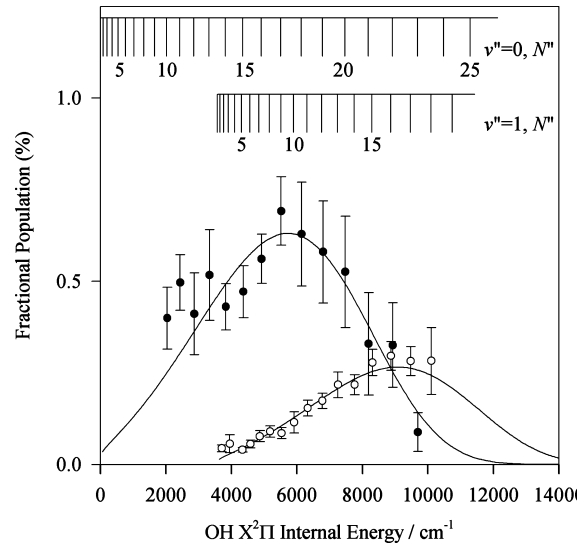

Figure 3. Nascent quantum state distribution of OH $X^2\Pi$ products arising from quenching of OH $A^2\Sigma^+$ ($v' = 0$, $N' = 0$) by O_2 under single-collision conditions. The fractional population of OH $X^2\Pi$ in $v'' = 0$ (●) and $v'' = 1$ (○) is shown with 1σ uncertainties derived from repeated intensity and fluorescence lifetime measurements. The population for each rotational state N'' represents the average of the four fine-structure components. The lines through the data are best fit functions used to interpolate the observed distributions to include unobserved quantum states, as described in the text.

However, previous studies comparing the rates of quenching and VET under thermal conditions show quenching to be nearly 10 times more efficient than VET for O_2.[40,41] Studies carried out with CO_2 showed that quenching is slightly more efficient than VET at high temperatures, although quenching becomes increasingly important at lower temperatures.[40] Consequently, electronic quenching is likely to provide the dominant contribution to the collisional removal rates for the OH $A^2\Sigma^+$ ($v' = 1$, N') levels reported here.

B. OH $X^2\Pi$ Product State Distributions. The OH $X^2\Pi$ PSDs from nonreactive quenching of OH $A^2\Sigma^+$ by O_2 and CO_2 have been measured under single-collision conditions. This is evident from the rate of collisional quenching over the 100 ns delay between the pump and probe lasers. Within this time period, less than one quenching collision occurs, as determined from the rate of collisional quenching, which is 0.003 ns^{-1} for O_2 and 0.004 ns^{-1} for CO_2. We also verified the attainment of single-collision conditions by doubling the delay between the pump and probe laser pulses and comparing the relative populations in selected OH $X^2\Pi$ product states. The relative populations were unchanged within experimental uncertainty, indicating that secondary collisions had not redistributed population in OH $X^2\Pi$.

The OH $X^2\Pi$ (v'', N'') PSDs generated from nonreactive quenching of OH $A^2\Sigma^+$ by O_2 and CO_2 are presented in Figures 3 and 4, respectively. The population for each rotational state N'' represents the average of the four fine-structure components. For both collision partners, the OH $X^2\Pi$ products are generated primarily in $v'' = 0$ with less population in $v'' = 1$. Despite a search covering a range of rotational and fine-structure levels of OH $X^2\Pi$ ($v'' = 2$), no products were detected for either collision partner. The distributions were also examined for fine-structure effects, which revealed that both Λ-doublet levels and F_1 and F_2 manifolds are equally populated within experimental uncertainty. Although the vibrational distributions and absence of fine-structure propensities are similar, the rotational distributions of the OH $X^2\Pi$ products from OH $A^2\Sigma^+$ quenching by

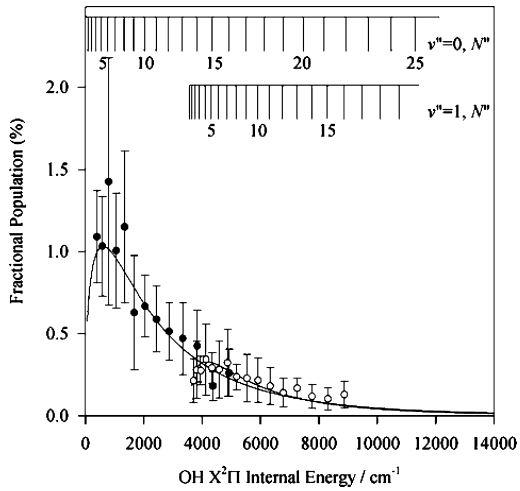

Figure 4. Nascent OH $X^2\Pi$ product state distribution arising from quenching of OH $A^2\Sigma^+$ ($v' = 0, N' = 0$) by CO_2 under single-collision conditions. The fractional population of OH $X^2\Pi$ in $v'' = 0$ (●) and $v'' = 1$ (○) is shown in an analogous manner as Figure 3; the lines through the data are best fit functions, as described in the text.

O_2 and CO_2 are significantly different from one another and are discussed separately below.

With O_2 as the collisional quenching partner, the OH $X^2\Pi$ products are highly rotationally excited (Figure 3). The product rotational distribution increases to a peak at $N'' \approx 17$, corresponding to ~5500 cm^{-1} of rotational energy, and then falls off at higher N''. A similar distribution is observed for $v'' = 1$ products. Population was detected in rotational levels as high as $N'' = 23$ in $v'' = 0$ and $N'' = 18$ in $v'' = 1$. Low N'' levels ($v'' = 0$, $N'' \leq 10$ and $v'' = 1$, $N'' \leq 2$) could not be detected above background signals (probe laser only) from jet-cooled OH $X^2\Pi$.

By contrast, quenching of OH $A^2\Sigma^+$ by CO_2 produces OH $X^2\Pi$ with more moderate rotational excitation (Figure 4). The rotational distribution peaks at low $N'' \approx 5$, corresponding to only ~600 cm^{-1} of rotational energy. The product distribution falls off gradually at higher N'', extending to $N'' = 16$ in $v'' = 0$ and $N'' = 17$ in $v'' = 1$. Again, the rotational distributions are equivalent for $v'' = 0$ and 1, and products in low N'' levels could not be detected above background.

A large number of OH $X^2\Pi$ product states were probed following quenching by O_2 and CO_2; nevertheless, the distributions are still incomplete. In some cases, individual states could not be probed in isolation because of spectral congestion; in others, small collision-induced populations, particularly in high rotational levels of $v'' = 0$ and 1, were below the detection limit. A complete OH $X^2\Pi$ product distribution is necessary to determine reliable average quantities as well as the overall branching between reactive and nonreactive quenching pathways.

To account for unobserved product states, we modeled the observed distributions using a Fisher−Tippett probability distribution, as had been done previously for quenching by H_2 and D_2.[42] A least-squares fitting procedure was then applied to fit the experimentally observed population distributions to

$$P(N'') = \frac{C \exp(-z - \exp(-z))}{\beta} \quad \text{where} \quad z = \frac{N'' - \alpha}{\beta} \tag{3}$$

In this function, the variable N'' is the rotational quantum number, C is a scaling constant, α is the peak of the distribution, and β is a measure of the breadth of the distribution. We stress that this function was selected for its simplicity and the goodness of fit to the experimental distributions, not for reasons of physical significance.

TABLE 1: Parameters Derived from Fits to the Experimental Data for the OH $X^2\Pi$ Products from Nonreactive Quenching of OH $A^2\Sigma^+$ by O_2 and CO_2[a]

	O_2	CO_2
α	17.3(3)	5.2(1.2)
β	4.2(2)	4.5(8)
$P(v'' = 0)$	0.28(1)	0.47(4)
$P(v'' = 1)$	0.12(1)	0.15(1)
$P(v'' \geq 2)$	0.09(1)	0.06(2)
$\langle E_{rot} \rangle / cm^{-1}$	4780(190)	1840(550)
Γ	0.40(1)	0.62(5)

[a] Parameters and associated uncertainties characterize the peak, α, and breadth, β, of the rotational distribution, the vibrational population distribution, $P(v'')$, and the mean rotational energy $\langle E_{rot} \rangle$. Γ is the branching fraction to OH $X^2\Pi$ ($v'' = 0$, 1) products from nonreactive quenching. $P(v'' \geq 2)$ is the estimated population in OH $X^2\Pi$ ($v'' \geq 2$) based on a surprisal analysis. (See the text for details.)

The three parameters characterizing the probability distribution (Table 1) were obtained as follows: We initially scaled the $v'' = 0$ and 1 distributions to each other by minimizing the root-mean-square deviation of populations between N'' levels common to both vibrational levels. The combined distribution was then fit to the Fisher−Tippett function to obtain values for the α and β parameters. This implicitly assumes that the $v'' = 0$ and 1 distributions have the same shape. With α and β fixed, the original distributions were then used to obtain two values of C. The mean rotational energy of the OH $X^2\Pi$ products is also determined from the fit parameters.

C. Branching Fraction for OH $X^2\Pi$ Products. Branching fractions for nonreactive quenching of OH $A^2\Sigma^+$ by O_2 and CO_2 were measured for two specific OH $X^2\Pi$ product channels with each collision partner. For O_2, the branching fraction was explicitly measured for quenching to the OH $X^2\Pi$ ($v'' = 1$, $N'' = 13$, F_1, e) and ($v'' = 1$, $N'' = 15$, F_1, f) product states. These measurements yielded Γ_i values of 0.16(3)% and 0.34(4)% for the $N'' = 13$, e and $N'' = 15$, f levels, respectively. The branching fraction measurements give a population ratio of 0.47(11) for $N'' = 13$, e compared with $N'' = 15$, f. This is in reasonable agreement with the relative populations obtained for these same two levels of 0.67(17). The branching fractions measured for the two specific product states were then used to convert the relative populations into fractional populations for the entire OH $X^2\Pi$ PSD, which are given in Figure 3. We obtained the overall branching fraction for nonreactive quenching, Γ, by summing the fractional populations determined from the fitting procedure described earlier over the rotational and fine-structure states in each vibrational level. Production of OH $X^2\Pi$ ($v'' = 0$) accounts for 28(1)% and ($v'' = 1$) for 12(1)% of the collisionally quenched OH $A^2\Sigma^+$, giving 40(1)% overall.

For CO_2, branching fractions were measured for quenching to the OH $X^2\Pi$ ($v'' = 1$, $N'' = 9$, F_1, e) and OH $X^2\Pi$ ($v'' = 1$, $N'' = 6$, F_1, f) product states. These measurements yielded Γ_i values of 0.28(8)% for $N'' = 9$, e and 0.29(3)% for $N'' = 6$, f and a population ratio 0.96(30) for $N'' = 9$, e compared with $N'' = 6$, f. Again, this is in agreement with the ratio of 0.86(76) obtained from relative population measurements. The larger uncertainty in the relative population measurements arises from difficulty in detecting products from quenching above background (probe laser only) from jet-cooled OH $X^2\Pi$. Scaling

the relative populations to fractional populations (Figure 4) and summing the OH $X^2\Pi$ PSDs over the rotational and fine-structure states indicates that 47(4)% of the products from quenching of OH $A^2\Sigma^+$ by CO_2 are formed in ($v'' = 0$) and 15(1)% in ($v'' = 1$), giving 62(5)% overall.

IV. Discussion

The OH $X^2\Pi$ PSDs and branching fractions following quenching of OH $A^2\Sigma^+$ by O_2 and CO_2 provide new insight into the dynamics of quenching collisions. OH $X^2\Pi$ ($v'' = 0$, 1) is produced with significant rotational excitation following quenching collisions with O_2 and a moderate degree of rotational excitation with CO_2. Branching fraction measurements, accompanied by modeling the population in unobserved levels, reveal that nonreactive quenching to produce OH $X^2\Pi$ ($v'' = 0$, 1) accounts for significant fractions of the total removal of OH $A^2\Sigma^+$ in collisions with O_2 and CO_2. These results will be discussed and compared with results obtained from analogous studies on quenching of OH $A^2\Sigma^+$ by H_2/D_2 and N_2[22,23,29,30] as well as quenching of NO $A^2\Sigma^+$ by O_2 and CO_2.[22,23,29,30,32,43,44]

The OH $X^2\Pi$ products from quenching by O_2 and CO_2 are primarily released in $v'' = 0$, with 2 to 3 times less population in $v'' = 1$. No population was detected in $v'' = 2$ with either collision partner. A vibrational surprisal analysis was carried out to estimate population in higher vibrational levels ($v'' \geq 2$) using known[45,46] and calculated[47] term values for OH $X^2\Pi$ and for O_2 and CO_2. This analysis reveals that both vibrational distributions are significantly colder than a prior distribution. From the surprisal analysis, we estimate that OH $X^2\Pi$ ($v'' \geq 2$) could account for a further 9(1)% of nonreactive products of quenching by O_2 and 6(2)% of products of quenching by CO_2. It is then somewhat surprising that we were unable to detect OH $X^2\Pi$ ($v'' = 2$) products. This suggests that $v'' = 2$ population may be spread over many rotational and fine-structure states, with the population in any particular OH $X^2\Pi$ ($v'' = 2$, N'', F_n, ε) product state below our detection limit. Alternatively, the opening of an additional pathway producing OH $X^2\Pi$ and electronically excited O_2 $a^1\Delta_g$ (7918 cm^{-1}) could potentially be more favorable than the production of OH $X^2\Pi$ ($v'' \geq 2$) + O_2 $X^3\Sigma_g^-$.

The limited vibrational excitation of the OH $X^2\Pi$ products is consistent with a spectator picture in which the OH bond length is perturbed very little despite there being sufficient energy available to populate levels up to $v'' = 12$. There is very little change in the OH bond length between the $A^2\Sigma^+$ and $X^2\Pi$ electronic states,[47] which would therefore favor "diagonal" ($\Delta v = 0$) transitions in the sudden limit, although we note that Franck−Condon models of quenching dynamics have been shown to have limited applicability[13,48] and have been challenged on theoretical grounds.[49] Similar OH $X^2\Pi$ product vibrational distributions were previously observed following quenching of OH $A^2\Sigma^+$ by H_2/D_2 and N_2; in all cases, the vibrational ground state is most populated. Ab initio calculations of the OH + H_2 system have shown that the minimum energy crossing point occurs with very little change in the OH bond length, which is consistent with the limited vibrational excitation observed in that system.[19,22] Quenching by other molecular partners appears to operate with similar constraints.

It is instructive to compare the observed OH $X^2\Pi$ vibrational distributions arising from nonreactive quenching of OH $A^2\Sigma^+$ by molecular collision partners with those measured for the analogous quenching of NO $A^2\Sigma^+$. Branching fractions for quenching of NO $A^2\Sigma^+(v' = 0)$ to NO $X^2\Pi$ ($v'' = 0$) with several molecular collision partners, including O_2 and CO_2, were measured in a flow cell using a time-resolved pump−probe method by Settersten et al.[32] It was found that O_2 resulted in a branching fraction to $v'' = 0$ of approximately 0.3, whereas CO_2 displayed a larger fraction of 0.6. The branching fractions determined in this work for quenching OH $A^2\Sigma^+$ ($v' = 0$) to OH $X^2\Pi$ ($v'' = 0$) are 0.28(1) with O_2 and 0.47(4) with CO_2, which is similar to what was observed for quenching of NO $A^2\Sigma^+$ by these molecular partners. It was inferred that the larger branching fraction for production of NO $X^2\Pi$ ($v'' = 0$) with CO_2 was due to an additional quenching channel that also produces NO $X^2\Pi$ ($v'' = 0$). Specifically, Settersten et al. proposed a mechanism in which quenching is accompanied by dissociation of CO_2 to CO $X^1\Sigma^+$ + O(^{3}P). Only NO $X^2\Pi$ ($v'' = 0$) can be produced in coincidence because of energetic constraints. CO products[32,43,44] arising from quenching of NO $A^2\Sigma^+$ by CO_2 have been detected, although the relative importance of this pathway is subject to significant uncertainty. The analogous pathway is not energetically allowed for quenching OH $A^2\Sigma^+$ ($v' = 0$) by CO_2. Therefore, the mechanism suggested for different branching fractions to $v'' = 0$ for quenching of NO $A^2\Sigma^+$ by O_2 and CO_2 is not the case for quenching of OH $A^2\Sigma^+$.

The rotational distribution of the OH $X^2\Pi$ products following quenching OH $A^2\Sigma^+$ by O_2 is highly nonthermal; this will be compared with the results from previously studied quenchers below. In contrast, the modest rotational excitation of OH $X^2\Pi$ products from quenching by CO_2 can be well characterized with a rotational temperature of 2250(90) K. This corresponds to an average rotational energy of 1630(30) cm^{-1}, which is in agreement with the mean rotational energy derived from the Fisher−Tippett fit to the PSD, 1840(550) cm^{-1} (Table 1). The thermal appearance of the OH $X^2\Pi$ rotational distribution suggests that energy redistribution occurs between the partners in the course of the quenching event, for example, through a long-lived collision complex. With CO_2, there are additional degrees of freedom that can accommodate the available energy. In particular, CO_2 has a denser manifold of rovibrational states that can be populated.

The extent of rotational excitation of the OH $X^2\Pi$ products also differs across the range of diatomic quenching partners examined to date. A high degree of rotational excitation is observed for the OH $X^2\Pi$ products following quenching by H_2/D_2, N_2, and O_2. The OH $X^2\Pi$ ($v'' = 0$) products from quenching by O_2 show less-extensive rotational excitation than those from quenching by N_2 with average rotational energies of 4830 and 6500 cm^{-1}, respectively; H_2 and D_2 quenchers result in somewhat less rotational excitation of OH $X^2\Pi$ with average rotational energies of 3680 and 4560 cm^{-1}, respectively. From a purely kinematic perspective in which the collision partner is assumed to be structureless, the degree of rotational excitation of the OH $X^2\Pi$ products from quenching would scale with the square root of the reduced mass of the system.[30] In this limit, rotational excitation of the OH $X^2\Pi$ products would follow because $O_2 > N_2 > D_2 > H_2$. This general trend had been observed for N_2, D_2, and H_2, but O_2 is found to be less effective than N_2 in generating rotational excitation of the OH $X^2\Pi$ products. This model neglects the structure of the collision partner and features of the potential energy surfaces, and thus it is entirely unsurprising that it fails. Another complicating aspect is the presence of many additional potential energy surfaces that correlate with OH $X^2\Pi$ + O_2 because of the triplet character of the ground $X^3\Sigma_g^-$ state and low-lying $a^1\Delta_g$, $b^1\Sigma_g^+$ electronic states of O_2. There is, however, no evidence of bimodality (or trimodality) in the OH $X^2\Pi$ PSD that could

indicate coincidental formation of different electronic states of O_2. It is also worthwhile to note that the OH $X^2\Pi$ products from quenching of OH $A^2\Sigma^+$ by O_2 and CO_2 show no fine-structure effects, whereas quenching by H_2/D_2 and N_2 showed a propensity for $\Pi(A')$ Λ-doublet levels that are indicative of $p\pi$ orbital alignment.[22,23,30] The lack of fine-structure effects suggests more extensive mixing of the excited state potential with the potentials derived from OH $X^2\Pi$ with O_2 and CO_2.

The branching fraction measurements for O_2 and CO_2 suggest that reactive quenching processes could also be significant. For quenching of OH $A^2\Sigma^+$ by O_2, 40(1)% of products have been identified as OH $X^2\Pi$ ($v'' = 0, 1$). Population from quenching in OH $X^2\Pi$ ($v'' = 0$, $N'' \leq 10$) could not be detected above background signals, suggesting that quenched population in these levels is small. The similarity of the shapes of the rotational distributions observed in $v'' = 0$ and 1 (for which lower N'' values were detected) also argues against any significant bimodality of the rotational distribution. The population from quenching in these unobserved levels is taken into account in the fitting procedure, which yields the percentage of products in OH $X^2\Pi$ ($v'' = 0, 1$). On the basis of the surprisal analysis, we estimate that OH $X^2\Pi$ ($v'' \geq 2$) could account for an additional 9(1)% of nonreactive quenching products The O_2 product can, in principle, be produced in any of its three lowest electronic states ($X\ ^3\Sigma_g^-$, $a^1\Delta_g$, $b^1\Sigma_g^+$), but we are unable to infer any information on relative populations from our experimental data. We anticipate that reaction accounts for the balance of quenching products.

Limiting the discussion to planar configurations, the interaction between OH $X^2\Pi$ and O_2 $X\ ^3\Sigma_g^-$ gives rise to states of $^2A''$, $^2A'$, $^4A''$, and $^4A'$ symmetry that correlate adiabatically with HO_2 $X^2A'' + O(^3P)$. However, states of $^2A''$ and $^4A''$ symmetry arise from the interaction of OH $A^2\Sigma^+$ with O_2 $X^3\Sigma_g^-$, and the latter correlates adiabatically with electronically excited HO_2 $A^2A' + O(^3P)$. The production of ground state HO_2 X^2A'' from OH $A^2\Sigma^+ + O_2$ $X^3\Sigma_g^-$ requires nonadiabaticity to be important. An alternative reaction channel is the production of O_3 $X^1A_1 + H(^2S)$. In planar configurations, however, this directly correlates with OH $X^2\Pi + O_2$ $X^3\Sigma_g^-$ on a surface of $^2A'$ symmetry. Again, this suggests that a nonadiabatic pathway would be required to access these reaction products. In future work, it would be desirable to characterize the products of reaction. The possible role of the HOOO intermediate is unknown.

Quenching of OH $A^2\Sigma^+$ by CO_2 results in 62(5)% of the products being OH $X^2\Pi$ ($v'' = 0, 1$) + CO_2. On the basis of the surprisal analysis, we estimate that an additional 6(2)% of quenching collisions result in the formation of OH $X^2\Pi$ ($v'' \geq 2$), although these products were not directly measured in these experiments. As for quenching by O_2, we presume that the remainder of quenching collisions lead to reaction. Energetically accessible reaction products are CO + HO_2 in either of its first two doublet states. For coplanar configurations, CO $X^1\Sigma^+$ + HO_2 X^2A'' and A^2A' correlate adiabatically with OH $X^2\Pi$ + CO_2. This suggests that a nonadiabatic pathway is needed to evolve from OH $A^2\Sigma^+ + CO_2$ to these reaction products.

The branching between nonreactive and reactive products differs greatly depending on the collision partner. For H_2 and D_2, only 12(5)% and 15(8)% of the quenched products are OH $X^2\Pi$ with the balance being lost through reaction.[29] For N_2, nonreactive quenching collisions dominate, with >88(3)% of the quenched population accounted for as OH $X^2\Pi$ and the balance thought most likely to be in yet higher undetected rotational states of $v'' = 0$ and 1.[30] Using O_2 and CO_2 as the collision partners, reactive and nonreactive quenching pathways are both found to be competitive. Ab initio calculations characterizing the topography of the CI are available for H_2 and N_2, and the branching fraction has been correlated with the tilt of the cone.[19,23,29] Characterization of the topography of any CI connecting the excited and ground state surfaces would be desirable for OH ($A^2\Sigma^+$, $X^2\Pi$) with O_2 and CO_2 and may help to provide a more general picture of the branching between nonreactive and reactive quenching for OH $A^2\Sigma^+$ with molecular collision partners. Quenching by CO_2 may occur by a different mechanism than the diatomic partners studied to date. In particular, the thermal appearance of the OH $X^2\Pi$ product rotational distribution suggests that quenching by CO_2 may proceed through a long-lived collision complex. Taken together, the OH $X^2\Pi$ PSDs and branching fraction measurements reported here are part of a larger body of work aimed at understanding the fundamental mechanism (or mechanisms) by which quenching occurs for OH $A^2\Sigma^+$ with molecular partners.

V. Conclusions

Comprehensive quantum state distributions for the OH $X^2\Pi$ products from quenching OH $A^2\Sigma^+$ ($v' = 0$, $N' = 0$) by O_2 and CO_2 are reported. For both collision partners, OH products are formed predominantly in $v'' = 0$ with less population in $v'' = 1$ and none detected in $v'' = 2$. No fine-structure effects are observed with either collision partner. With O_2 as the collision partner, the ground-state OH $X^2\Pi$ products are generated with a significant degree of rotational excitation, peaking at $N'' \approx 17$ with $\sim$4800 cm^{-1} of rotational energy on average. Branching fraction measurements reveal that 40(1)% of the products are OH $X^2\Pi$ ($v'' = 0, 1$). With CO_2 as the collision partner, OH $X^2\Pi$ radicals are produced with a more moderate degree of rotational excitation, peaking at $N'' \approx 5$ with an average rotational energy of $\sim$1800 cm^{-1}. In the case of quenching by CO_2, 62(5)% of the products are identified as OH $X^2\Pi$ ($v'' = 0, 1$). For both systems, the balance may be found in higher OH $X^2\Pi$ vibrational levels $v'' \geq 2$ or reactive quenching channels.

These results differ from previous observations made using H_2/D_2 and N_2 collision partners. In particular, quenching by O_2 and CO_2 show markedly different branching for the production of OH $X^2\Pi$. The observations made using H_2/D_2 and N_2 collision partners were supplemented by ab initio theoretical calculations of the interaction potential between the collision partner and OH in its electronic ground $X^2\Pi$ and excited $A^2\Sigma^+$ states. Such calculations would be extremely useful in understanding the underlying dynamics of the quenching process for O_2 and CO_2. Experimental studies determining the quantum state distribution of the O_2 or CO_2 product of nonreactive quenching events would provide a fuller picture of the quenching process. Additionally, further experimental work characterizing the reaction products from energetically available quenching pathways is highly desired for both systems.

Acknowledgment. This research has been supported by the Office of Basic Energy Sciences of the Department of Energy.

References and Notes

(1) Finlayson-Pitts, B. J.; Pitts, J. N. *Chemistry of the Upper and Lower Atmosphere: Theory, Experiments, and Applications*; Academic: San Diego, 1999.

(2) Glassman, I. *Editor Combustion*, 3rd ed.; Academic Press: London, 1996.

(3) Crosley, D. R. Laser Fluorescence Detection of Atmospheric Hydroxyl Radicals. In *Progress and Problems in Atmospheric Chemistry*; Barker, J. R., Ed.; World HScientific Publishing Company: Singapore, 1995; Vol. 3, pp 256.

(4) Copeland, R. A.; Dyer, M. J.; Crosley, D. R. *J. Chem. Phys.* **1985**, *82*, 4022.

(5) Hemming, B. L.; Crosley, D. R.; Harrington, J. E.; Sick, V. *J. Chem. Phys.* **2001**, *115*, 3099.

(6) Hemming, B. L.; Crosley, D. R. *J. Phys. Chem. A* **2002**, *106*, 8992.

(7) German, K. R. *J. Chem. Phys.* **1976**, *64*, 4065.

(8) Burris, J.; Butler, J. J.; McGee, T. J.; Heaps, W. S. *Chem. Phys.* **1988**, *124*, 251.

(9) Burris, J.; Butler, J.; McGee, T.; Heaps, W. *Chem. Phys.* **1991**, *151*, 233.

(10) Bailey, A. E.; Heard, D. E.; Paul, P. H.; Pilling, M. J. *J. Chem. Soc., Faraday Trans.* **1997**, *93*, 2915.

(11) Copeland, R. A.; Crosley, D. R. *J. Chem. Phys.* **1986**, *84*, 3099.

(12) Fairchild, P. W.; Smith, G. P.; Crosley, D. R. *J. Chem. Phys.* **1983**, *79*, 1795.

(13) Dagdigian, P. J. *Annu. Rev. Phys. Chem.* **1997**, *48*, 95.

(14) Asscher, M.; Haas, Y. *J. Chem. Phys.* **1982**, *76*, 2115.

(15) Paul, P. H.; Carter, C. D.; Gray, J. A.; Durant, J. L., Jr.; Furlanetto, M. R. *Correlations for the OH $A^2\Sigma^+$ ($v' = 0$) Electronic Quenching Cross-Section*; Sandia National Laboratories: Livermore, CA, 1994.

(16) Paul, P. H. *J. Quant. Spectrosc. Radiat. Transfer* **1994**, *51*, 511.

(17) Bailey, A. E.; Heard, D. E.; Henderson, D. A.; Paul, P. H. *Chem. Phys. Lett.* **1999**, *302*, 132.

(18) Schatz, G. C.; Fisher, B.; Grande, W.; Kumayama, K.; Pederson, L. A. *J. Phys. Chem. A* **2001**, *105*, 2515.

(19) Hoffman, B. C.; Yarkony, D. R. *J. Chem. Phys.* **2000**, *113*, 10091.

(20) Lester, M. I.; Loomis, R. A.; Schwartz, R. L.; Walch, S. P. *J. Phys. Chem. A* **1997**, *101*, 9195.

(21) Yarkony, D. R. *J. Chem. Phys.* **1999**, *111*, 6661.

(22) Cleary, P. A.; Dempsey, L. P.; Murray, C.; Lester, M. I.; Kłos, J.; Alexander, M. H. *J. Chem. Phys.* **2007**, *126*, 204316.

(23) Dempsey, L. P.; Sechler, T. D.; Murray, C.; Lester, M. I.; Matsika, S. *J. Chem. Phys.* **2009**, *130*, 104307.

(24) Anderson, D. T.; Todd, M. W.; Lester, M. I. *J. Chem. Phys.* **1999**, *110*, 11117.

(25) Todd, M. W.; Anderson, D. T.; Lester, M. I. *J. Phys. Chem. A* **2001**, *105*, 10031.

(26) Ortiz-Suárez, M.; Witinski, M. F.; Davis, H. F. *J. Chem. Phys.* **2006**, *124*, 201106.

(27) Estupiñán, E. G.; Stickel, R. E.; Wine, P. H. *Chem. Phys. Lett.* **2001**, *336*, 109.

(28) Pollack, I. B.; Lei, Y. X.; Stephenson, T. A.; Lester, M. I. *Chem. Phys. Lett.* **2006**, *421*, 324.

(29) Dempsey, L. P.; Murray, C.; Lester, M. I. *J. Chem. Phys.* **2007**, *127*, 151101.

(30) Dempsey, L. P.; Murray, C.; Cleary, P. A.; Lester, M. I. *Phys. Chem. Chem. Phys.* **2008**, *10*, 1424.

(31) Hancock, G.; Saunders, M. *Phys. Chem. Chem. Phys.* **2008**, *10*, 2014.

(32) Settersten, T. B.; Patterson, B. D.; Kronemayer, H.; Sick, V.; Schulz, C.; Daily, J. W. *Phys. Chem. Chem. Phys.* **2006**, *8*, 5328.

(33) Yarkony, D. R. *Acc. Chem. Res.* **1998**, *31*, 511.

(34) Sander, S. P.; Finlayson-Pitts, B. J.; Friedl, R. R.; Golden, D. M.; Huie, R. E.; Keller-Rudek, H.; Kolb, C. E.; Kurylo, M. J.; Molina, M. J.; Moortgat, G. K.; Orkin, V. L.; Ravishankara, A. R.; Wine, P. H. *Chemical Kinetics and Photochemical Data for Use in Atmospheric Studies, Evaluation Number 15*; JPL Publication 06-2; Jet Propulsion Laboratory: Pasadena, CA, 2006.

(35) Derro, E. L.; Sechler, T. D.; Murray, C.; Lester, M. I. *J. Chem. Phys.* **2008**, *128*, 244313.

(36) Derro, E. L.; Murray, C.; Sechler, T. D.; Lester, M. I. *J. Phys. Chem. A* **2007**, *111*, 11592.

(37) Murray, C.; Derro, E. L.; Sechler, T. D.; Lester, M. I. *J. Phys. Chem. A* **2007**, *111*, 4727.

(38) Suma, K.; Sumiyoshi, Y.; Endo, Y. *Science* **2005**, *308*, 1885.

(39) Luque, J.; Crosley, D. R. SRI International Report MP 99-0091999.

(40) Steffens, K. L.; Crosley, D. R. *J. Chem. Phys.* **2000**, *112*, 9427.

(41) Williams, L. R.; Crosley, D. R. *J. Chem. Phys.* **1996**, *104*, 6507.

(42) *Handbook of Mathematical Functions with Formulas, Graphs, and Mathematical Tables*; Abramowitz, M.; Stegun, I., Eds.; Dover Publications: New York, 1972.

(43) Cohen, N.; Heicklen, J. *J. Phys. Chem.* **1967**, *71*, 558.

(44) Zhao, G. B.; Hu, X. D.; Argyle, M. D.; Radosz, M. *Ind. Eng. Chem. Res.* **2005**, *44*, 3925.

(45) Colin, R.; Coheur, P.-F.; Kiseleva, M.; Vandaele, A. C.; Bernath, P. F. *J. Mol. Spectrosc.* **2002**, *214*, 225.

(46) Copeland, R. A.; Chalamala, B. R.; Coxon, J. A. *J. Mol. Spectrosc.* **1993**, *161*, 243.

(47) Huber, K. P.; Herzberg, G. Constants of Diatomic Molecules (Data Prepared by J.W. Gallagher and R.D. Johnson III). In *NIST Chemistry WebBook*; NIST Standard Reference Database Number 69; National Institute of Standards and Technology: Gaithersburg, MD, 2008. http://webbook.nist.gov.

(48) McKendrick, K. G. *J. Chem. Soc., Faraday Trans.* **1998**, *94*, 1921.

(49) Alexander, M. H.; Corey, G. C. *J. Chem. Phys.* **1986**, *84*, 100.

JP902935C